PHYSICAL REVIEW D **93,** 114512 (2016)

$K \to \pi$ semileptonic form factors with $N_f = 2 + 1 + 1$ twisted mass fermions

N. Carrasco,[1] P. Lami,[2,1] V. Lubicz,[2,1] L. Riggio,[1] S. Simula,[1] and C. Tarantino[2,1]
(ETM Collaboration)

[1]*INFN, Sezione di Roma Tre Via della Vasca Navale 84, I-00146 Rome, Italy*
[2]*Dipartimento di Matematica e Fisica, Università degli Studi Roma Tre Via della Vasca Navale 84, I-00146 Rome, Italy*

(Received 18 February 2016; published 20 June 2016)

We present a lattice QCD determination of the vector and scalar form factors of the semileptonic $K \to \pi \ell \nu$ decay which are relevant for the extraction of the Cabibbo-Kobayashi-Maskawa matrix element $|V_{us}|$ from experimental data. Our results are based on the gauge configurations produced by the European Twisted Mass Collaboration with $N_f = 2 + 1 + 1$ dynamical fermions, which include in the sea, besides two light mass degenerate quarks, also the strange and the charm quarks. We use data simulated at three different values of the lattice spacing and with pion masses as small as 210 MeV. Our final result for the vector form factor at zero momentum transfer is $f_+(0) = 0.9709(46)$, where the uncertainty is both statistical and systematic combined in quadrature. Using the latest experimental value of $f_+(0)|V_{us}|$ from $K_{\ell 3}$ decays, we obtain $|V_{us}| = 0.2230(11)$, which allows us to test the unitarity constraint of the Standard Model below the permille level once the determination of $|V_{ud}|$ from superallowed nuclear β decays is adopted. A slight tension with unitarity at the level of ~ 2 standard deviations is observed. Moreover, we present our results for the semileptonic scalar $f_0(q^2)$ and vector $f_+(q^2)$ form factors in the whole range of values of the squared four-momentum transfer q^2 measured in $K_{\ell 3}$ decays, obtaining a very good agreement with the momentum dependence of the experimental data. We provide a set of synthetic data points representing our results for the vector and scalar form factors at the physical point for several selected values of q^2.

DOI: 10.1103/PhysRevD.93.114512

I. INTRODUCTION

In the Standard Model (SM) of particle physics, the relative strength of the flavor-changing weak quark currents is parametrized by the unitary Cabibbo-Kobayashi-Maskawa (CKM) matrix [1], which provides the only source of CP violation in the quark sector. The unitarity of the CKM matrix implies various relations between its matrix elements, known as the unitarity triangles. The goal of flavor physics experiments is the measurement of the angles and sides of the unitarity triangles as well as the determination of many redundant observables sensitive to the CKM matrix elements. The consistency of such a plethora of measurements would be spoiled by possible deviations from the SM, signalling the presence of New Physics (NP). Therefore, an accurate determination of the CKM matrix elements is crucial both for testing the SM and for searching NP.

Let us focus on the determination of the Cabibbo's angle, or equivalently the CKM matrix element $|V_{us}|$, which enters both the leptonic kaon ($K_{\ell 2}$) decays via the axial quark current and the semileptonic kaon ($K_{\ell 3}$) decays via the vector quark current [2]. According to the $V - A$ structure of the SM weak current, the decay rate of both processes should provide the same result for $|V_{us}|$, once the relevant hadronic quantities, namely the ratio of the kaon and pion leptonic decay constants f_K/f_π and the semileptonic vector form factor at zero four-momentum transfer $f_+(0)$, are determined starting from our fundamental theory of the strong interactions, i.e., from QCD. As is well known, such a task can be properly carried out by simulating QCD on a lattice.

The history of the efforts in predicting both f_K/f_π and $f_+(0)$ using lattice QCD (LQCD) is nicely summarized in the recent reviews [3,4] of the Flavor Lattice Averaging Group (FLAG). As far as the form factor $f_+(0)$ is concerned, the first attempt to calculate it on the lattice dates back to the work of Ref. [5], which was performed in the quenched approximation ($N_f = 0$) with simulated pions not lighter than $\simeq 500$ MeV. Since then, several improvements have been achieved, and the most important ones are the inclusion of the effects of the loops of dynamical sea quarks, thanks to the production of unquenched gauge ensembles with $N_f = 2$, $2 + 1$ and $2 + 1 + 1$ sea quarks, and the simulation of lighter pions, which have recently reached the physical point [6,7]. Only one calculation of $f_+(0)$ exists to date [6] with four flavors of dynamical quarks ($N_f = 2 + 1 + 1$), which include in the sea, besides two light mass degenerate quarks, also the strange and the charm quarks.

In this work, we present a new LQCD prediction of the form factor $f_+(0)$ obtained using the ensembles of gauge configurations produced by the European Twisted Mass (ETM) Collaboration with $N_f = 2 + 1 + 1$ dynamical

TABLE I. Values of the simulated sea and valence quark bare masses, of the pion (M_π) and kaon (M_K) masses, of the lattice size L and of the product $M_\pi L$ for the various gauge ensembles used in this work. The values of M_K given for each gauge ensemble do not correspond to the value of the simulated strange bare mass shown in the seventh column but to a renormalized strange mass interpolated at the physical value $m_s = 99.6(4.3)$ MeV [14].

Ensemble	β	V/a^4	$a\mu_{\rm sea} = a\mu_\ell$	$a\mu_\sigma$	$a\mu_\delta$	$a\mu_s$	M_π (MeV)	M_K (MeV)	L (fm)	$M_\pi L$
*A*30.32	1.90	$32^3 \times 64$	0.0030	0.15	0.19	$\{0.0145, 0.0185, 0.0225\}$	275	577	2.84	3.96
*A*40.32			0.0040				315	588		4.53
*A*50.32			0.0050				350	595		5.04
*A*40.24		$24^3 \times 48$	0.0040				324	594	2.13	3.50
*A*60.24			0.0060				388	610		4.19
*A*80.24			0.0080				438	624		4.73
*A*100.24			0.0100				497	650		5.37
*B*25.32	1.95	$32^3 \times 64$	0.0025	0.135	0.170	$\{0.0141, 0.0180, 0.0219\}$	259	553	2.61	3.43
*B*35.32			0.0035				300	562		3.97
*B*55.32			0.0055				377	587		4.99
*B*75.32			0.0075				437	608		5.78
*B*85.24		$24^3 \times 48$	0.0085				463	617	1.96	4.60
*D*15.48	2.10	$48^3 \times 96$	0.0015	0.12	0.1385	$\{0.0118, 0.0151, 0.0184\}$	224	538	2.97	3.37
*D*20.48			0.0020				255	541		3.84
*D*30.48			0.0030				310	554		4.67

quarks [8,9]. Furthermore, we have evaluated the strangeness changing vector $f_+(q^2)$ and scalar $f_0(q^2)$ form factors in the whole range of values of the squared four-momentum transfer q^2 measured in $K_{\ell 3}$ decays, obtaining a very good agreement with the momentum dependence of the experimental data [2,10]. Preliminary results have been already presented in Refs. [11–13].

The gauge ensembles and the simulations used in this work are the same as those adopted in Ref. [14] to determine the up, down, strange and charm quark masses (see Tables 1–3 of Ref. [14]), using the experimental value of the pion decay constant, f_π, to set the lattice scale,[1] as well as in Ref. [15] to calculate the ratio of leptonic decay constants f_K/f_π. The gauge fields are simulated using the Iwasaki gluon action [16], while sea quarks are implemented with the Wilson twisted mass action at maximal twist [17,18]. In order to avoid the mixing of strange and charm quarks in the valence sector, we have adopted the nonunitary setup described in Ref. [19], in which the valence strange quarks are regularized as Osterwalder-Seiler fermions [20], while the valence up and down quarks have the same action of the sea. The strange and charm mixing can occur in the hadronic decomposition of correlation functions only when the valence strange and charm quarks are regularized using the same twisted-mass doublet adopted for the strange and charm sea quarks (see Eq. (8) of Ref. [14]). The use of different lattice regularizations for valence and sea heavy quarks avoids completely the effects of flavor mixing without modifying the renormalization pattern of operators in massless schemes and produces only a modification of discretization effects. Moreover, since we work at maximal twist (i.e., we impose that the bare Wilson mass is tuned at its critical value, which is common to all the different quarks), an automatic $\mathcal{O}(a)$ improvement [18,19] is guaranteed also for our nonunitary setup.

The simulations have been carried out at three different values of the inverse bare lattice coupling β to allow for a controlled extrapolation to the continuum limit and different lattice volumes. For each gauge ensemble, we have used a number of gauge configurations corresponding to a separation of 20 trajectories to avoid autocorrelations. For the light sector, we have simulated quark masses in the range from $3m_{ud}$ to $12m_{ud}$ and for the strange sector from $0.7m_s$ to $1.2m_s$, where m_{ud} and m_s are the physical values of the (renormalized) average up/down and strange quark masses, respectively, as determined in Ref. [14]. The lattice spacings are found to be $a = \{0.0885(36), 0.0815(30), 0.0619(18)\}$ fm at $\beta = \{1.90, 1.95, 2.10\}$, respectively; the lattice volume goes from $\simeq 2$ to $\simeq 3$ fm; and the pion masses, extrapolated to the continuum and infinite volume limits, range from $\simeq 210$ to $\simeq 450$ MeV (see later Table I and Ref. [14] for further details).

We present our study of the semileptonic $K \to \pi$ form factors using the results of the eight branches of the analysis carried out in Ref. [14] for determining the up, down, strange and charm quark masses. The various branches differ by (i) the choice of the scaling variable, which was taken to be either the Sommer parameter r_0/a [21] or the mass of a fictitious pseudoscalar (PS) meson made of two strangelike quarks $aM_{s's'}$; (ii) the fitting procedures, which were based either on chiral perturbation theory (ChPT) or on a polynomial expansion in the light-quark mass (for the

[1]With respect to Ref. [14], the number of independent gauge configurations adopted for the ensemble D15.48 has been increased to 90 to improve the statistics.

motivations, see the discussion in Sec. 3.1 of Ref. [14]); and (iii) the choice between two methods, denoted as M1 and M2, which differ by $\mathcal{O}(a^2)$ effects (see, e.g., Ref. [22]), used to determine nonperturbatively the values of the mass renormalization constant (RC) $Z_m = 1/Z_P$ [14]. Throughout this work, the results corresponding to the various branches of the analysis are combined to form our average and error according to Eq. (28) of Ref. [14].

The final results for the form factor $f_+(0)$ and the CKM matrix element $|V_{us}|$ we present in this paper are

$$f_+(0) = 0.9709(46), \qquad |V_{us}| = 0.2230(11). \quad (1)$$

Once the determinations of $|V_{ud}|$ from superallowed nuclear β decays [23] and of $|V_{ub}|$ from B-meson decays [24] are adopted, the unitarity test of the first row of the CKM matrix becomes

$$\begin{aligned} |V_{ud}|^2 + |V_{us}|^2 + |V_{ub}|^2 &= 0.99875(41)_{V_{ud}}(49)_{V_{us}} \\ &= 0.99875(64), \end{aligned} \quad (2)$$

which highlights a slight tension with unitarity at the level of ~ 2 standard deviations. Note also that the total uncertainty in the rhs of Eq. (2) is below the permille level and the contribution due to the error on $|V_{us}|$ is comparable with the one related to $|V_{ud}|$.

As for the q^2-dependence of the semileptonic vector $f_+(q^2)$ and scalar $f_0(q^2)$ form factors, the same dispersive parametrization used to describe the experimental data [2,10] has been adopted to fit our results extrapolated to the physical point. The dispersive fit depends on two parameters, Λ_+ and C, which represent, respectively, the slope of the vector form factor $f_+(q^2)$ at $q^2 = 0$ (in units of M_π^2) and the scalar form factor $f_0(q^2)$ at the (unphysical) Callan-Treiman (CT) point $q^2 = q^2_{\rm CT} \equiv M_K^2 - M_\pi^2$ [25] divided by $f_+(0)$. Our final results are

$$\begin{aligned} \Lambda_+ &= 24.22(1.16) \times 10^{-3}, \\ \log(C) &= 0.1998(138), \end{aligned} \quad (3)$$

which compare positively with the latest experimental results [10]

$$\begin{aligned} \Lambda_+^{\rm exp} &= 25.75(36) \times 10^{-3}, \\ \log(C)^{\rm exp} &= 0.1985(70). \end{aligned} \quad (4)$$

The physics described by our simulations and used throughout this work corresponds to the isospin symmetric limit of QCD, where $m_u = m_d = m_{ud}$, assuming also zero quark electric charges. Therefore, isospin breaking and electromagnetic corrections have to be added separately in phenomenological analyses (see, e.g., Ref. [2]).

The paper is organized as follows. In Sec. II, we present the computational strategies adopted to extract the semileptonic form factors $f_+(q^2)$ and $f_0(q^2)$ from the two- and three-point correlation functions evaluated on the lattice using both the vector and scalar strangeness changing quark currents. In Secs. III and IV, we present our results at the physical point and in the continuum limit coming from two different strategies. The first one is based on the study of the momentum dependence of the form factors $f_+(q^2)$ and $f_0(q^2)$ to obtain the form factor $f_+(0)$ at each simulated light-quark mass m_ℓ and then to extrapolate the results for $f_+(0)$ to the physical point $m_\ell = m_{ud}$ and to the continuum limit. The second strategy uses a combined fit of the q^2, m_ℓ and lattice spacing dependencies of our form factor data, obtaining in this way the momentum dependence of the form factors at the physical point for both spacelike and timelike q^2. We provide a set of synthetic data points representing our results for $f_+(q^2)$ and $f_0(q^2)$ at the physical point for several selected values of q^2, including also the covariance matrix for the data at different values of q^2. We compare our results with the experimental data, obtaining a very good agreement in the whole range of values of q^2 measured in $K_{\ell 3}$ decays. In Sec. V, we present our determination of the CKM matrix element $|V_{us}|$, and we test the unitarity of the first row of the CKM matrix. Our conclusions are summarized in Sec. VI.

II. LATTICE COMPUTATION OF THE FORM FACTORS

The matrix element of the strangeness changing vector current $\hat{V}^\mu$ between kaon and pion states decomposes into two form factors, f_+ and f_-, as

$$\begin{aligned} \langle \hat{V}_\mu \rangle &\equiv \langle \pi(p_\pi)|\hat{V}_\mu|K(p_K)\rangle \\ &= (p_K + p_\pi)_\mu f_+(q^2) + (p_K - p_\pi)_\mu f_-(q^2), \end{aligned} \quad (5)$$

where $q_\mu = (p_K - p_\pi)_\mu$ is the 4-momentum transferred between the kaon and the pion.

The scalar form factor f_0 is defined as

$$f_0(q^2) \equiv f_+(q^2) + \frac{q^2}{M_K^2 - M_\pi^2} f_-(q^2) \quad (6)$$

and satisfies by definition the relation $f_+(0) = f_0(0)$. The form factor f_0 is proportional to the 4-divergence of $\langle \hat{V}_\mu \rangle$, which in turn, thanks to the vector Ward-Takahashi identity, is related to the matrix element of the strangeness changing scalar density $\hat{S}$ between kaon and pion states, leading to

$$\langle \hat{S} \rangle \equiv \langle \pi(p_\pi)|\hat{S}|K(p_K)\rangle = \frac{M_K^2 - M_\pi^2}{m_s - m_{ud}} f_0(q^2). \quad (7)$$

Equations (5) and (7) represent a system of redundant relations between the two form factors $f_+(q^2)$ and $f_0(q^2)$

and the matrix elements $\langle \hat{V}_\mu \rangle$ and $\langle \hat{S} \rangle$. The latter can be determined by studying the time dependence of suitable combinations of (Euclidean) two- and three-point correlation functions, namely

$$C_2^{\pi(K)}(t';\vec{p}_{\pi(K)}) = \frac{1}{L^3}\sum_{\vec{x},\vec{z}} \langle 0|P_5^{\pi(K)}(x)P_5^{\pi(K)\dagger}(z)|0\rangle \times e^{-i\vec{p}_{\pi(K)}\cdot(\vec{x}-\vec{z})}\delta_{t',(t_x-t_z)}, \quad (8)$$

$$C_{\hat{\Gamma}}^{K\pi}(t,t';\vec{p}_K,\vec{p}_\pi) = \frac{1}{L^6}\sum_{\vec{x},\vec{y},\vec{z}} \langle 0|P_5^{\pi}(x)\hat{\Gamma}(y)P_5^{K\dagger}(z)|0\rangle \times e^{-i\vec{p}_K\cdot(\vec{y}-\vec{z})+i\vec{p}_\pi\cdot(\vec{y}-\vec{x})}\delta_{t,(t_y-t_z)}\delta_{t',(t_x-t_z)}, \quad (9)$$

where t' is the time distance between the source and the sink, t is the time distance between the insertion of the current $\Gamma \in \{\hat{V}_\mu, \hat{S}\}$ and the source, and $P_5^\pi(x) = i\overline{u}(x)\gamma_5 d(x)$ and $P_5^K(x) = i\overline{s}(x)\gamma_5 d(x)$ are the (local) interpolating fields of the pion and kaon mesons. In our lattice setup, the Wilson parameters of the two valence quarks in any PS meson are always chosen to have opposite values, i.e., $r_s = r_u = -r_d$. In this way, the squared PS mass differs from its continuum counterpart only by terms of $\mathcal{O}(a^2 m)$ [18].

The statistical accuracy of the correlators (8)–(9) can be significantly improved by using the all-to-all quark propagators evaluated with the so-called "one-end" stochastic method [26], which includes spatial stochastic sources at a single time slice chosen randomly (see Ref. [27], where the degenerate case of the pion is illustrated in details). Statistical errors are always evaluated using the jackknife procedure, while cross-correlations are taken into account by the use of the eight bootstrap samplings corresponding to the eight analyses of Ref. [14] summarised in Sec. I. In Table I, we summarize the basic simulation parameters as well as the pion and kaon masses corresponding to each ensemble used in this work.

At large values of the time distances t, t' and $(t'-t)$, one has

$$C_2^{\pi(K)}(t';\vec{p}\pi(K)) \xrightarrow[t'\gg a]{} \frac{|Z_{\pi(K)}|^2}{2E_{\pi(K)}}[e^{-E_{\pi(K)}t'} + e^{-E_{\pi(K)}(T-t')}], \quad (10)$$

$$C_{\hat{\Gamma}}^{K\pi}(t,t';\vec{p}_K,\vec{p}_\pi) \xrightarrow[t,t',(t'-t)\gg a]{} \frac{Z_\pi Z_K^*}{4E_\pi E_K}\langle \pi(p_\pi)|\hat{\Gamma}|K(p_K)\rangle e^{-E_K t}e^{-E_\pi(t'-t)}, \quad (11)$$

where $E_{\pi(K)}$ is the pion (kaon) energy and $Z_{\pi(K)} \equiv \langle 0|P_5^{\pi(K)}(0)|\pi(K)\rangle$ is independent on the pion (kaon) momentum up to discretization effects. Using the exponential fit given by the rhs of Eq. (10), the pion and kaon energies can be extracted directly from the corresponding two-point correlation functions. The time intervals $[t_{\rm min}, t_{\rm max}]$ adopted for the fit (10) can be read off from Table 4 of Ref. [14]. We have checked that (i) the changes in the meson energies due to a decrease in the value of $t_{\rm min}$ by one or two lattice units are well below the statistical uncertainty and (ii) the extracted values of $E_{\pi(K)}$ are nicely reproduced (within statistical errors) by the continuumlike dispersive relation $E^{\rm disp}_{\pi(K)} = \sqrt{M^2_{\pi(K)} + |\vec{p}_{\pi(K)}|^2}$, where $M_{\pi(K)}$ is the meson mass extracted from the two-point correlator corresponding to the meson at rest.

In our lattice setup, we employs maximally twisted fermions, and therefore the vector $\hat{V}_\mu$ and the scalar $\hat{S}$ currents renormalize multiplicatively [18]. Introducing the local bare currents $V_\mu(x) \equiv \overline{s}(x)\gamma_\mu u(x)$ and $S(x) \equiv \overline{s}(x)u(x)$ and keeping the same value for the Wilson parameters of the initial and final quarks (i.e., $r_s = r_u$), one has

$$\hat{V}_\mu(x) = Z_V V_\mu(x) = Z_V \overline{s}(x)\gamma_\mu u(x), \quad (12)$$

$$\hat{S}(x) = Z_P S(x) = Z_P \overline{s}(x)u(x), \quad (13)$$

where Z_V and Z_P are the RCs of the vector and pseudoscalar densities for standard Wilson fermions, respectively, determined using the RI'-MOM method in Ref. [14]. The twisted quark masses renormalize multiplicatively with a RC Z_m given by $Z_m = 1/Z_P$ [18], which means that the product $(m_s - m_{ud})\langle \hat{S} \rangle$ does not depend on the RC Z_P. Therefore, according to Eq. (7), the scalar form factor $f_0(q^2)$ is related to the (bare) matrix element $\langle S \rangle$ by

$$\langle S \rangle \equiv \langle \pi(p_\pi)|S|K(p_K)\rangle = \frac{M_K^2 - M_\pi^2}{\mu_s - \mu_\ell} f_0(q^2), \quad (14)$$

where μ_ℓ and μ_s are the light and strange bare quark masses, respectively.

The (renormalized) matrix elements $\langle \hat{V}_\mu \rangle$ can be extracted from the time dependence of suitable ratios $R_\mu^{(V)}$ of the three-point correlation functions, defined as in Eq. (9) but using the local bare current $V_\mu(x)$, namely for $\mu = 0, 1, 2, 3$,

$$R_\mu^{(V)}(t;\vec{p}_K,\vec{p}_\pi) \equiv 4p_{K\mu}p_{\pi\mu}\frac{C_{V_\mu}^{K\pi}(t,\frac{T}{2};\vec{p}_K,\vec{p}_\pi)C_{V_\mu}^{\pi K}(t,\frac{T}{2};\vec{p}_\pi,\vec{p}_K)}{C_{V_\mu}^{\pi\pi}(t,\frac{T}{2};\vec{p}_\pi,\vec{p}_\pi)C_{V_\mu}^{KK}(t,\frac{T}{2};\vec{p}_K,\vec{p}_K)}, \quad (15)$$

where the time distance between the source and the sink has been fixed[2] at $t' = T/2$. We point out that the denominator of Eq. (15) is simply the numerator evaluated in the mass-degenerate limit for the valence quarks in the current.

[2]This choice allows us to improve the statistics by averaging the correlation functions between the two halves of the time extension of the lattice.

Denoting the bare masses of the quarks in the current as (μ_1, μ_2), the two correlation functions in the numerator correspond to (μ_s, μ_ℓ) and (μ_ℓ, μ_s), respectively, while the denominator refers to the cases (μ_ℓ, μ_ℓ) and (μ_s, μ_s). Though mass-degenerate, the current quarks in the denominator have the same lattice regularizations of the corresponding quarks in the numerator. Thus, the same RC Z_V is present at the numerator and denominator, and it cancels out in the ratio.

At large time distances t, a plateau is expected to occur, viz.

$$R_\mu^{(V)}(t;\vec{p}_K,\vec{p}_\pi) \xrightarrow[t\gg a,(T/2-t)\gg a]{} 4p_{K\mu}p_{\pi\mu}\frac{\langle\pi(p_\pi)|\hat{V}_\mu|K(p_K)\rangle\langle K(p_K)|\hat{V}_\mu|\pi(p_\pi)\rangle}{\langle\pi(p_\pi)|\hat{V}_\mu|\pi(p_\pi)\rangle\langle K(p_K)|\hat{V}_\mu|K(p_K)\rangle}, \tag{16}$$

which, we stress, does not depend on the RC Z_V and on the matrix elements Z_π and Z_K of the interpolating PS fields. Moreover, thanks to charge conservation, one has $\langle\pi(p_\pi)|\hat{V}_\mu|\pi(p_\pi)\rangle = 2p_{\pi\mu}$ and $\langle K(p_K)|\hat{V}_\mu|K(p_K)\rangle = 2p_{K\mu}$ up to lattice artifacts, and therefore the plateau of $R_\mu^{(V)}(t;\vec{p}_K,\vec{p}_\pi)$ at large time distances provides directly the quantity $|\langle\hat{V}_\mu\rangle|^2$. Taking the square root, the absolute value of the matrix element $\langle\hat{V}_\mu\rangle$ is obtained, while the sign of $\langle\hat{V}_\mu\rangle$ can be easily inferred from the sign of the plateau of the ratio $C_{V_\mu}^{K\pi}(t,\frac{T}{2};\vec{p}_K,\vec{p}_\pi)/[C_2^K(t;\vec{p}_K)C_2^\pi(T/2-t;\vec{p}_\pi)]$ at large time distances.

Note that when a spatial component of either the pion or the kaon momentum is vanishing, the corresponding matrix element $\langle\pi(p_\pi)|V_i|\pi(p_\pi)\rangle$ or $\langle K(p_K)|V_i|K(p_K)\rangle$ $(i = 1, 2, 3)$ is also vanishing and cannot be used in the denominator of the rhs of Eq. (15). In these cases, the quantity $2p_{\pi i}/\langle\pi(p_\pi)|V_i|\pi(p_\pi)\rangle$ (or $2p_{Ki}/\langle K(p_K)|V_i|K(p_K)\rangle$) is replaced in Eq. (15) by $2E_\pi/\langle\pi(p_\pi)|V_0|\pi(p_\pi)\rangle$ (or $2E_K/\langle K(p_K)|V_0|K(p_K)\rangle$).

In the case of both a pion and kaon at rest, only the time component $R_0^{(V)}$ can be constructed providing a quite precise determination of the scalar form factor $f_0(q^2)$ at kinematical end point $q^2 = q^2_{\rm max} \equiv (M_K - M_\pi)^2$, namely [5]

$$R_0^{(V)}(t;\vec{p}_K=\vec{0},\vec{p}_\pi=\vec{0}) \xrightarrow[t\gg a,(T/2-t)\gg a]{} [(M_K+M_\pi)f_0(q^2_{\rm max})]^2. \tag{17}$$

In our present simulations, Eq. (17) allows us to achieve a precision for $f_0(q^2_{\rm max})$ ranging from $\simeq 0.02\%$ to $\simeq 0.5\%$ (see Table III).

In the case of the scalar density, we investigate the time dependence of a suitable double ratio $R^{(S)}$ of two- and three-point correlation functions, defined in terms of the local bare density $S(x)$ as

$$R^{(S)}(t;\vec{p}_K,\vec{p}_\pi) \equiv 16E_KE_\pi\frac{C_S^{K\pi}(t,\frac{T}{2};\vec{p}_K,\vec{p}_\pi)C_S^{\pi K}(t,\frac{T}{2};\vec{p}_\pi,\vec{p}_K)}{C_2^K(T/2;\vec{p}_K)C_2^\pi(T/2;\vec{p}_\pi)}. \tag{18}$$

At large time distances t, one gets

$$R^{(S)}(t;\vec{p}_K,\vec{p}_\pi) \xrightarrow[t\gg a,(T/2-t)\gg a]{} |\langle\pi(p_\pi)|S|K(p_K)\rangle|^2, \tag{19}$$

which provides directly the (bare) quantity $|\langle S\rangle|^2$ independently on the matrix elements Z_π and Z_K of the interpolating PS fields. As in the case of the vector current, taking the square root of $R^{(S)}$, the absolute value of the matrix element $\langle S\rangle$ can be obtained, while the sign of $\langle S\rangle$ can be easily inferred from the sign of the plateau of the ratio $C_S^{K\pi}(t,\frac{T}{2};\vec{p}_K,\vec{p}_\pi)/[C_2^K(t;\vec{p}_K)C_2^\pi(T/2-t;\vec{p}_\pi)]$ at large time distances.

When both the pion and kaon are at rest, Eq. (18) provides a determination of $f_0(q^2_{\rm max})$, which turns out to be significantly less precise than the one obtained from Eq. (17), i.e., using the vector current. Moreover, at variance with Eq. (15), where only ratios of three-point correlation functions appear, the definition (18) involves ratios of three- to two-point functions, which typically are less correlated with each other. Thus, in order both to make use of three-point functions only and to take advantage of the statistically precise quantity $R_0^{(V)}(t;\vec{0},\vec{0})$, we introduce a new *scalar* ratio $\overline{R}^{(S)}$, which combines three-point correlators corresponding to both scalar and vector quark currents, defined as

$$\overline{R}^{(S)}(t;\vec{p}_K,\vec{p}_\pi) \equiv \overline{K}R_0^{(V)}(t;\vec{0},\vec{0})\frac{C_S^{K\pi}(t,\frac{T}{2};\vec{p}_K,\vec{p}_\pi)C_S^{\pi K}(t,\frac{T}{2};\vec{p}_\pi,\vec{p}_K)}{C_S^{K\pi}(t,\frac{T}{2};\vec{0},\vec{0})C_S^{\pi K}(t,\frac{T}{2};\vec{0},\vec{0})}, \tag{20}$$

where $\overline{K}$ is a simple kinematical factor depending on meson and quark masses, namely

$$\overline{K} = \left[\frac{M_K - M_\pi}{\mu_s - \mu_\ell}\frac{E_KE_\pi}{M_KM_\pi}\right]^2 e^{(E_K-M_K+E_\pi-M_\pi)\dot{T}/2}. \tag{21}$$

At large time distances t, one gets again (up to lattice artifacts which may differ from those of the ratio $R^{(S)}$)

$$\overline{R}^{(S)}(t;\vec{p}_K,\vec{p}_\pi) \xrightarrow[t\gg a,(T/2-t)\gg a]{} |\langle\pi(p_\pi)|S|K(p_K)\rangle|^2. \tag{22}$$

The use of Eq. (20) improves significantly the statistical precision of the extracted matrix element $\langle S\rangle$ with respect to the case of Eq. (18), as it is illustrated in Fig. 1. The improvement in the precision may reach even a factor larger than 2.

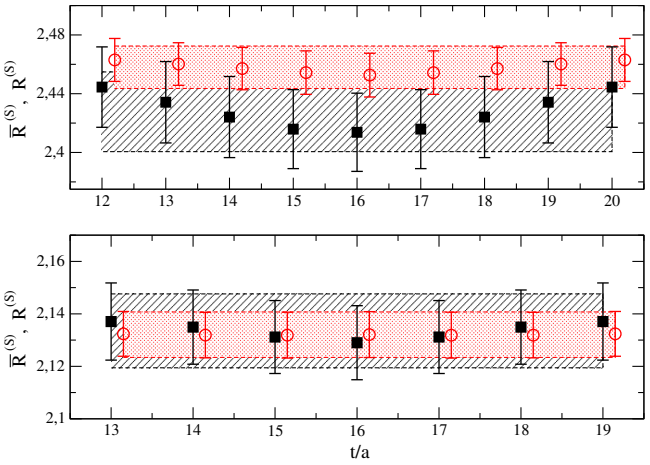

FIG. 1. Double ratios $R^{(S)}$ (black squares) and $\bar{R}^{(S)}$ (red dots), given by Eqs. (18) and (20), respectively, vs the Euclidean time t/a in the cases of the ensembles A30.32 with $a\mu_s = 0.0185$ (upper panel) and B55.32 with $a\mu_s = 0.0180$ (lower panel). The meson masses are $(M_\pi, M_K) \simeq (275, 510)$ MeV (upper panel) and $(M_\pi, M_K) \simeq (375, 545)$ MeV (lower panel). The values of the pion and kaon momentum correspond to $|\vec{p}_K| = 0$ and $|\vec{p}_\pi| \simeq 150$ MeV for both panels. The black and red areas correspond to the values of the extracted matrix element $|\langle \pi(p_\pi)|S|K(p_K)\rangle|^2$ obtained using the plateau regions described later in the text and shown in the figure. The corresponding values of the squared 4-momentum transfer q^2 are close to $q^2 = 0$, namely $q^2 \simeq 0.016$ GeV^2 (upper panel) and $q^2 \simeq -0.003$ GeV^2 (lower panel).

In lattice QCD simulations the spatial components of the hadronic momenta p_j $(j = 1, 2, 3)$ are quantized. The specific values depend on the choice of the boundary conditions (BCs) applied to the quark fields. References [28,29] proposed using (partially) twisted BCs for the (valence) quark fields,

$$\psi(x + \hat{e}_j L) = e^{2\pi i \theta_j} \psi(x), \tag{23}$$

which allow shifting the quantized values of p_j by an arbitrary amount equal to $2\pi\theta_j/L$, namely

$$p_j = \theta_j \frac{2\pi}{L} + n_j \frac{2\pi}{L}, \tag{24}$$

where the n_j's are integer numbers. Such a choice is crucial for removing the strong limitations to the kinematical regions accessible for the investigation of momentum dependent quantities (like, e.g., form factors), imposed by the use of periodic BCs (i.e., $\theta_j = 0$). In Refs. [30,31], it was shown that the momentum shift produced by the partially twisted BCs does not introduce any additional noise and allows determining the form factors of the $K_{\ell 3}$ decays with good accuracy for both spacelike and timelike 4-momentum transfer q^2.

The partially twisted BCs can be tuned to determine the $K_{\ell 3}$ form factors directly at the relevant kinematical point $q^2 = 0$ [32,33], avoiding in this way the need for an Ansatz with which to perform the q^2-interpolation of the form factor data.[3] Such a direct strategy has been used in the recent computations of $f_+(0)$ performed by the FNAL/MILC [6] and RBC/UKQCD [7] collaborations. In this work, instead, we study the momentum dependence of both the scalar and vector form factors in order to compare it with the experimental data, while profiting at the same time from the high precision achievable for the scalar form factor near the kinematical end point $q^2 = q^2_{\rm max}$ (see Refs. [5,30,34]). Note in particular that, thanks to the use of the new ratio (20), the high-precision determination of $f_0(q^2_{\rm max})$ from the vector quark current improves significantly the evaluation of the scalar form factor $f_0(q^2)$ from the scalar density also at $q^2 \simeq 0$ (see Fig. 1).

According to Ref. [18], the matrix elements $\langle \hat{V}_\mu \rangle$ and $\langle S \rangle$ can be $\mathcal{O}(a)$ improved by averaging the two kinematics with opposite spatial momenta of the initial and final mesons, namely

$$\langle \hat{V}_0 \rangle_{imp} \equiv \frac{1}{2}[\langle \pi(E_\pi, \vec{p}_\pi)|\hat{V}_0|K(E_K, \vec{p}_K)\rangle + \langle \pi(E_\pi, -\vec{p}_\pi)|\hat{V}_0|K(E_K, -\vec{p}_K)\rangle], \tag{25}$$

$$\langle \hat{V}_i \rangle_{imp} \equiv \frac{1}{2}[\langle \pi(E_\pi, \vec{p}_\pi)|\hat{V}_i|K(E_K, \vec{p}_K)\rangle - \langle \pi(E_\pi, -\vec{p}_\pi)|\hat{V}_i|K(E_K, -\vec{p}_K)\rangle], \tag{26}$$

$$\langle S \rangle_{imp} \equiv \frac{1}{2}[\langle \pi(E_\pi, \vec{p}_\pi)|S|K(E_K, \vec{p}_K)\rangle + \langle \pi(E_\pi, -\vec{p}_\pi)|S|K(E_K, -\vec{p}_K)\rangle]. \tag{27}$$

The effect of the above averages turns out to be quite mild (within the statistical errors) in the case of both the time component of the vector current and the scalar density, while it is found to be significant for the matrix elements of the spatial components of the vector current.

We impose on the valence quark fields twisted BCs in the spatial directions and antiperiodic BCs in time. On the other hand, the ETM Collaboration gauge configurations have been produced by including in the sea dynamical quarks with periodic BCs in space and antiperiodic ones in time. It has been shown [35,36] that for physical quantities, which do not involve final state interactions (like, e.g., meson masses, decay constants, semileptonic form factors and electromagnetic transitions), the use of different BCs for

[3]The systematic uncertainty related to the choice of the Ansatz for the q^2-interpolation turns out, however, to be a subdominant effect (see Ref. [34] and later Sec. III).

TABLE II. Values of the parameter θ appearing in Eq. (28) chosen for the various ETM Collaboration gauge ensembles with $N_f = 2+1+1$ adopted in this work.

β	V/a^4	θ
1.90	$24^3 \times 48$	$\{-0.350, -0.150, 0.0, 0.150, 0.350\}$
1.90	$32^3 \times 64$	$\{-0.467, -0.200, 0.0, 0.200, 0.467\}$
1.95	$24^3 \times 48$	$\{-0.321, -0.138, 0.0, 0.138, 0.321\}$
1.95	$32^3 \times 64$	$\{-0.427, -0.183, 0.0, 0.183, 0.427\}$
2.10	$48^3 \times 96$	$\{-0.493, -0.212, 0.0, 0.212, 0.493\}$

valence and sea quarks is legitimate, since it produces finite volume effects which are exponentially small.

Thus, generalizing Eq. (23) to four dimensions, we introduce the 4-vector θ_μ given by

$$\theta_\mu = \left(\frac{L}{T}\theta_0, \theta_1, \theta_2, \theta_3\right) = \left(\frac{L}{2T}, \theta, \theta, \theta\right), \qquad (28)$$

where the values of θ adopted for the various gauge ensembles are collected in Table II. They have been chosen in order to provide approximately the same physical values of the quark spatial momenta $\vec{p} = (2\pi/L)(\theta, \theta, \theta)$ at the various lattice spacings and volumes. In addition, the opposite values of θ allow us to perform the averages of Eqs. (25)–(27), achieving in this way the $\mathcal{O}(a)$-improvement for the matrix elements.

For the calculation of the relevant three-point correlation functions $C^{K\pi}_{V_\mu}(t, \frac{T}{2}; \vec{p}_K, \vec{p}_\pi)$ and $C^{K\pi}_{S}(t, \frac{T}{2}; \vec{p}_K, \vec{p}_\pi)$, we consider the spectator d-quark at rest and apply the partially twisted BCs (28) to the initial s- and final u-quarks. In this way, the kaon and pion momentum are given by $\vec{p}_K = (2\pi/L)(\theta_K, \theta_K, \theta_K)$ and $\vec{p}_\pi = (2\pi/L)(\theta_\pi, \theta_\pi, \theta_\pi)$, where θ_K and θ_π assume the values of the parameter θ given in Table II for each gauge ensemble.

Since we are using spatially symmetric twisted BCs, the matrix elements of the spatial components of the vector current $\langle \hat{V}_i \rangle_{imp}$ are equal to each other. Therefore, in order to improve the statistics, we average them to get

$$\langle \hat{V}_{sp} \rangle_{imp} = \frac{1}{3}[\langle \hat{V}_1 \rangle_{imp} + \langle \hat{V}_2 \rangle_{imp} + \langle \hat{V}_3 \rangle_{imp}]. \qquad (29)$$

The nice quality of the plateaux for the matrix elements $\langle \hat{V}_0 \rangle_{imp}$, $\langle \hat{V}_{sp} \rangle_{imp}$ and $\langle S \rangle_{imp}$ is illustrated in Fig. 2. The time intervals adopted for the fits (16) and (22) are symmetric around $T/4a$ and equal to (10–14) for $T/a = 48$, (12–20) for $T/a = 64$ at $\beta = 1.90$, (13)–(19) for $T/a = 64$ at $\beta = 1.95$ and (18)–(30) for $T/a = 96$. These values are compatible with the dominance of the pion and kaon ground state observed in the two-point correlation functions in Ref. [14]. We have also checked that the more conservative choice $[T/4a - 2, T/4a + 2]$ for the lattices with time extension $T/a = 64$ and 96 yields changes in the extracted matrix elements well below the statistical uncertainty.[4]

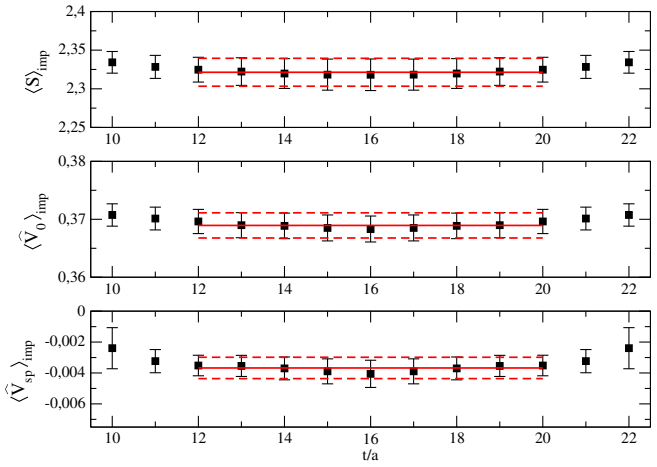

FIG. 2. Matrix elements $\langle \hat{V}_{sp} \rangle_{imp}$, $\langle \hat{V}_0 \rangle_{imp}$ and $\langle S \rangle_{imp}$ extracted from the ratios R_μ and $\bar{R}_S$ [see Eqs. (15) and (20)] for the ensemble A40.32 with $\beta = 1.90$, $L/a = 32$, $a\mu_l = 0.0040$, $a\mu_s = 0.0185$, $\vec{p}_K = -\vec{p}_\pi$ and $|\vec{p}_K| \simeq 150$ MeV. The meson masses are $M_\pi \simeq 315$ MeV and $M_K \simeq 525$ MeV. The horizontal red lines correspond to the plateau regions used to extract the matrix elements and to their central values and statistical errors (see the text).

To sum up, from the two-point and three-point lattice correlators, we determine three $\mathcal{O}(a)$-improved matrix elements, namely $\langle \hat{V}_0 \rangle_{imp}$, $\langle \hat{V}_{sp} \rangle_{imp}$ and $\langle S \rangle_{imp}$, which are related to the scalar $f_0(q^2)$ and vector $f_+(q^2)$ form factors by the redundant system of relations given by

$$\langle \hat{V}_0 \rangle_{imp} = (E_K + E_\pi) f_+(q^2) + (E_K - E_\pi)\frac{M_K^2 - M_\pi^2}{q^2} \times [f_0(q^2) - f_+(q^2)] + \mathcal{O}(a^2), \qquad (30)$$

$$\hat{V}_{sp} \rangle_{imp} = \frac{2\pi}{L}\left\{(\theta_K + \theta_\pi) f_+(q^2) + (\theta_K - \theta_\pi) \times \frac{M_K^2 - M_\pi^2}{q^2}[f_0(q^2) - f_+(q^2)]\right\} + \mathcal{O}(a^2), \qquad (31)$$

$$\langle S \rangle_{imp} = \frac{M_K^2 - M_\pi^2}{\mu_s - \mu_\ell} f_0(q^2) + \mathcal{O}(a^2). \qquad (32)$$

We determine the form factors $f_0(q^2)$ and $f_+(q^2)$ by minimizing the χ^2-variable constructed using the three Eqs. (30)–(32).

[4]Excited states may contaminate the double ratios (16) and (22) in a t-independent way. However, in the case of the ratio $C^{K\pi}_{\hat{\Gamma}}(t, t'; \vec{p}_K, \vec{p}_\pi)/C^K_2(t; \vec{p}_K)C^\pi_2(t' - t; \vec{p}_\pi)$, the contaminations are t dependent, since the excited states from the source and the sink are different. We have checked that for the above ratio, the quality of the plateaux is similar to the one shown in Figs. 1 and 2.

After a small interpolation of our lattice data to the physical value of the strange quark mass $m_s = 99.6(4.3)$ MeV, determined in Ref. [14], we present in the next sections our results at the physical point and in the continuum limit coming from two different strategies.

The first strategy is based on the study of the momentum dependence of the form factors $f_0(q^2)$ and $f_+(q^2)$ using either the z-expansion of Ref. [37] or a polynomial fit. In this way, we determine the form factor $f_+(0)$ at each simulated value of the (renormalized) light-quark mass m_ℓ. Then, the results obtained for $f_+(0)$ are extrapolated to the physical point $m_\ell = m_{ud}$ and to the continuum limit using either SU(2) [38] or SU(3) [39,40] ChPT predictions.

The second strategy, inspired by our previous work [41] done with the $N_f = 2$ ETM Collaboration gauge ensembles, is based on a combined fit of the q^2, m_ℓ and lattice spacing dependencies of our lattice data for the form factors $f_0(q^2)$ and $f_+(q^2)$ together with the result for the ratio of the kaon and pion leptonic decay constants f_K/f_π obtained at the chiral point in Ref. [15]. The latter quantity is used for imposing the constraint coming from the Callan-Treiman theorem [25]. In this way, the momentum dependence of the form factors $f_0(q^2)$ and $f_+(q^2)$ is obtained, at the physical point, in the whole range of values of q^2 measured in $K_{\ell 3}$ decays [2,10], i.e., from $q^2 = 0$ up to the physical end point $q^2 = q^2_{\rm max} \simeq 0.129$ GeV^2.

III. FIRST STRATEGY: INTERPOLATION OF THE FORM FACTORS AT $q^2 = 0$

In the first strategy, for each gauge ensemble, we fit simultaneously our lattice data for $f_{+,0}(q^2)$ using the z-expansion as parametrized in Ref. [37], namely

$$f_{+,0}(q^2) = \frac{a^{(0)}_{+,0} + a^{(1)}_{+,0}(z + \frac{1}{2}z^2)}{1 - \frac{q^2}{M^2_{V,S}}}, \tag{33}$$

where $a^{(0)}_{+,0}$, $a^{(1)}_{+,0}$, M_V and M_S (representing the vector and scalar pole masses, respectively) are kept as free parameters and z is defined as

$$z = \frac{\sqrt{t_+ - q^2} - \sqrt{t_+ - t_0}}{\sqrt{t_+ - q^2} + \sqrt{t_+ - t_0}} \tag{34}$$

with t_+ and t_0 given by

$$t_+ = (M_K + M_\pi)^2,$$
$$t_0 = (M_K + M_\pi)(\sqrt{M_K} - \sqrt{M_\pi})^2. \tag{35}$$

The condition $f_+(0) = f_0(0)$ is imposed by rewriting Eq. (33) in the form

$$f_{+,0}(q^2) = \frac{f_+(0) + a^{(1)}_{+,0}(z - z_0)[1 + (z + z_0)/2]}{1 - q^2/M^2_{V,S}}, \tag{36}$$

where $z_0 \equiv z(q^2 = 0)$, reducing in this way the number of free parameters to five for each gauge ensemble.

We also fit the q^2-dependence of the form factors using an alternative, simple Ansatz (a quadratic fit in q^2), obtaining nearly identical results, as can be seen in the left panel of Fig. 3. The q^2-range of our lattice data includes the timelike region $0 < q^2 < q^2_{\rm max}$ as well as the spacelike one, reaching quite large negative values of q^2. Since concerns may be raised about the size of lattice artifacts at large negative values of q^2, which correspond to large values of the quark momenta [32], we have either included or excluded in our fits the data corresponding to large negative values of q^2 (corresponding to $a^2q^2 < -0.01$). Again, nearly identical results are obtained, as is shown in the right panel of Fig. 3.

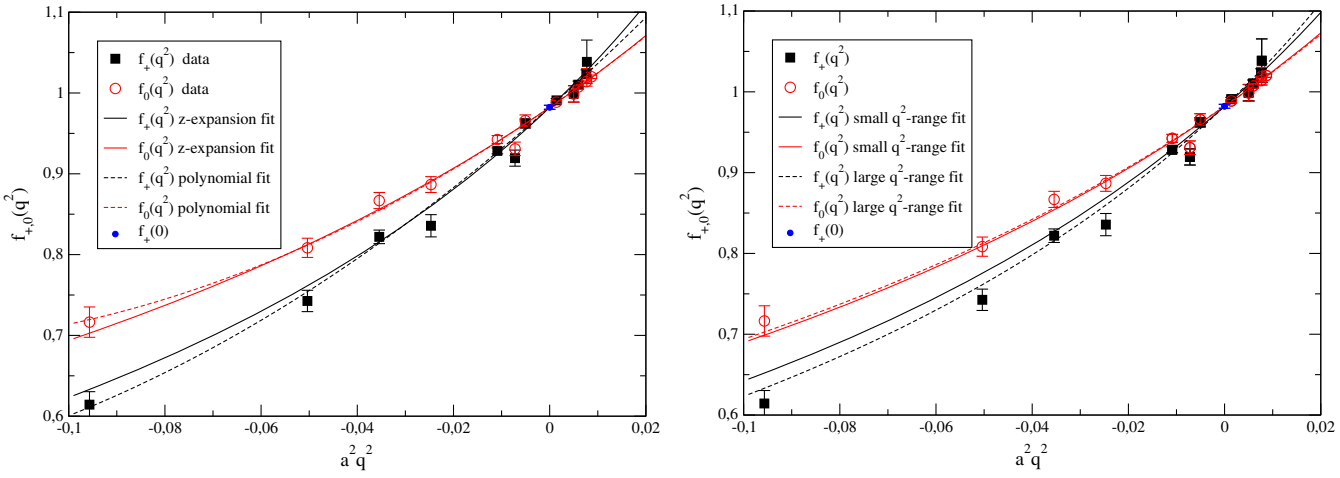

FIG. 3. Left panel: results of the fit of our lattice data for the form factors $f_+(q^2)$ and $f_0(q^2)$ using the z-expansion (continuum lines), given by Eq. (36), compared to the ones obtained adopting a simple quadratic formula in q^2 (dashed lines). Right panel: z-expansion fit of the form factors using only the data corresponding to $a^2q^2 > -0.01$ (continuum lines) or using all the data (dashed lines). Both panels correspond to the ensemble A60.24 with $\beta = 1.90$, $L/a = 24$, $a\mu_\ell = 0.0060$ and $a\mu_s = 0.0185$.

TABLE III. Values of the scalar form factor $f_0(q^2_{\rm max})$ at the kinematical end point $q^2_{\rm max} = (M_K - M_\pi)^2$ and of the form factor $f_+(0) = f_0(0)$, obtained using the z-expansion (36) or a simple quadratic fit in q^2, vs the (renormalized) light-quark mass m_ℓ for each gauge ensemble used in this work. The (renomalized) strange quark mass has been interpolated at the physical value $m_s =$ 99.6(4.3) MeV [14].

Ensemble	β	V/a^4	$a\mu_{\rm sea} = a\mu_\ell$	m_ℓ(MeV)	$f_0(q^2_{\rm max})$	$f_+(0)$ (z-expansion)	$f_+(0)$ (quadratic)
*A*30.32	1.90	$32^3 \times 64$	0.0030	12.1	1.0397(19)	0.9792(28)	0.9804(27)
*A*40.32			0.0040	16.2	1.0250(28)	0.9767(32)	0.9774(31)
*A*50.32			0.0050	20.2	1.0109(13)	0.9813(15)	0.9808(15)
*A*40.24	1.90	$24^3 \times 48$	0.0040	16.2	1.0269(32)	0.9801(28)	0.9802(26)
*A*60.24			0.0060	24.2	1.0101(12)	0.9870(16)	0.9865(16)
*A*80.24			0.0080	32.3	1.0025(04)	0.9924(04)	0.9922(04)
*A*100.24			0.0100	40.4	1.0005(03)	0.9969(04)	0.9969(03)
*B*25.32	1.95	$32^3 \times 64$	0.0025	11.5	1.0486(35)	0.9772(50)	0.9767(51)
*B*35.32			0.0035	16.1	1.0222(20)	0.9808(28)	0.9810(28)
*B*55.32			0.0055	25.3	1.0095(07)	0.9910(12)	0.9906(13)
*B*75.32			0.0075	34.5	1.0028(04)	0.9938(10)	0.9938(10)
*B*85.24	1.95	$24^3 \times 48$	0.0085	39.1	1.0012(2)	0.9963(02)	0.9964(03)
*D*15.48	2.10	$48^3 \times 96$	0.0015	9.0	1.0567(55)	0.9833(84)	0.9841(83)
*D*20.48			0.0020	12.0	1.0400(32)	0.9842(42)	0.9844(46)
*D*30.48			0.0030	18.1	1.0162(16)	0.9870(24)	0.9863(26)

The results for $f_+(0)$ obtained using the z-expansion or the quadratic fit in q^2 are collected in Table III for each value of the (renormalized) light-quark mass. It can clearly be seen that the values of $f_+(0)$ corresponding to the two different Ansätze for the q^2-dependence differ by less than $1/4$ of the statistical errors, which represents therefore a subdominant effect (see also Ref. [34]). Notice also that (i) the two lattice points calculated at the same lattice spacing and light-quark mass but different volumes (corresponding to the ensembles A40.24 and A40.32) are compatible within 1 standard deviation and (ii) finite size effects (FSEs) are expected to be maximal for the ensemble A40.24, having the coarsest lattice spacing with the smallest pion mass and lattice volume (see Ref. [14]).

In order to compute the physical value of the form factor $f_+(0)$, we perform the extrapolation to the physical point using both SU(2) [38] and SU(3) ChPT predictions [39,40].

For the SU(2) ChPT Ansatz, we use

$$f_+(0) = F_+\left[1 - \frac{3}{4}\xi \log \xi + C_1\xi + C_2\xi^2 + D(a/r_0)^2\right], \tag{37}$$

where $\xi_\ell \equiv 2Bm_\ell/16\pi^2 f^2$ with B and f being the SU(2) low-energy constants (LECs) entering the leading-order chiral Lagrangian and determined in Ref. [14], while the quantities F_+, C_1, C_2 and D are free fitting parameters. In Eq. (37), we have added quadratic terms in ξ, $C_2\xi^2$ and, in the lattice spacing, $D_+(a/r_0)^2$, in order to take into account next-to-next-to-leading order (NNLO) ChPT and $\mathcal{O}(a)$-improved discretization effects, respectively.

The SU(3) ChPT expansion of the form factor $f_+(0)$ reads as

$$f_+(0) = 1 + f_2 + \Delta f, \tag{38}$$

where the next-to-leading-order (NLO) term f_2 does not depend on any NLO LEC and it can be written in terms of meson masses, namely [39,40]

$$f_2 = \frac{3}{2}H_{\pi K} + \frac{3}{2}H_{\eta K}, \tag{39}$$

with

$$H_{PQ} = -\frac{1}{64\pi^2 f^2}\left[M_P^2 + M_Q^2 + \frac{2M_P^2 M_Q^2}{M_P^2 - M_Q^2}\log\frac{M_Q^2}{M_P^2}\right]. \tag{40}$$

In Eq. (38), the quantity Δf represents NNLO contributions and beyond, which we parametrize in our fit as

$$\Delta f = \left(\frac{M_K^2 - M_\pi^2}{M_K^2}\right)^2 [\Delta_0 + \Delta_1\xi + \Delta_2(a/r_0)^2], \tag{41}$$

where $\Delta_{0,1,2}$ are free parameters. Equations (38)–(41) verify the constraint imposed by the Ademollo-Gatto theorem [42] at any value of the lattice spacing, i.e., deviations of $f_+(0)$ from unity are at least quadratic in the SU(3)-breaking parameter $(M_K^2 - M_\pi^2) \propto (m_s - m_\ell)$. We tried also an alternative Ansatz for Δf in which the Ademollo-Gatto theorem is satisfied only in the continuum limit, namely $\Delta f = [\tilde{\Delta}_0 + \tilde{\Delta}_1\xi](M_K^2 - M_\pi^2)^2/M_K^4 + \tilde{\Delta}_2(a/r_0)^2$, obtaining, however, a fit of poorer quality to the lattice data.

Notice that (i) in the SU(3) fit of our lattice data the strange quark mass is fixed at its physical value and (ii) in Eq. (40) the pion decay constant f at the chiral point can be replaced by its value f_π at the physical point. The

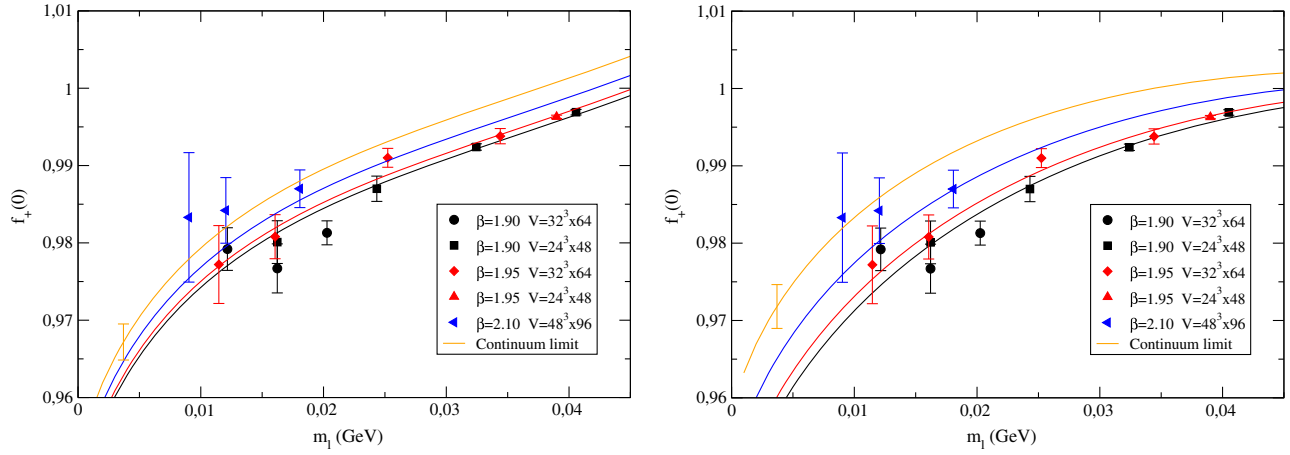

FIG. 4. Chiral and continuum extrapolation of $f_+(0)$ based on the SU(2) ChPT fit given by Eq. (37) (left) and on the SU(3) ChPT fit given by Eqs. (38)–(41) (right).

difference is a NNLO effect that should be reabsorbed by Δf. We have verified that the final result for $f_+(0)$ at the physical point is almost independent on the precise choice of the pion decay constant f appearing in Eq. (40), once Eq. (41) is included in the fit.

The chiral and continuum extrapolations of $f_+(0)$ are shown in Fig. 4 for both the SU(2) and SU(3) fits. Combining the two analyses, we get our result for the vector form factor $f_+(0)$ at the physical point and in the continuum limit,

$$f_+(0) = 0.9697(45)_{\text{stat+fit}}(11)_{\text{input}}(25)_{\text{syst}} = 0.9697(52), \tag{42}$$

where $()_{\text{stat+fit}}$ indicates the statistical uncertainty which includes also the one induced by the fitting procedure, while $()_{\text{input}}$ takes into account the uncertainties present in the determination of the input parameters [14], namely the values of the average u/d quark mass m_{ud}, the lattice spacing a and the SU(2) ChPT low energy constants f and B. The systematic uncertainty, indicated as $()_{\text{syst}}$, is dominated by the chiral extrapolation error, estimated as half of the difference of the results corresponding to the SU(2) and SU(3) ChPT extrapolations. The discretization error has been estimated by comparing with the results obtained, including in Eqs. (37) and (41) a term proportional to $(a/r_0)^4$ (adopting for the coefficient a prior equal to 0 ± 3), and turns out to be below the permille level.

Before closing this section, we note that for each bootstrap event, we use the uncorrelated χ^2-variable for our fits. The χ^2 is not used to estimate the errors on the fitting parameters, which are always evaluated with the boostrap procedure, in which correlations are automatically taken into account. Since part of the uncertainties in our fits has also a systematic origin, like the distribution of the input parameters in the analyses carried out in Ref. [14], the χ^2-distribution is not fully significant in order to quantify the quality of the extrapolations. Indeed, the goodness-of-fit tests would require statistical errors only. Nevertheless, we note that the values of χ^2 in the various fits carried out for the chiral and continuum extrapolations turn out to be comparable. This is the reason why we combine the results corresponding to the various branches of the analysis with the same weight, according to Eq. (28) of Ref. [14].

IV. SECOND STRATEGY: COMBINED FIT

In this section, we present the results of our second strategy in which we extrapolate the form factors $f_+(q^2)$ and $f_0(q^2)$ to the physical point for a wide range of values of q^2, which includes the q^2-region accessible to experiments, i.e., from $q^2 = 0$ to the kinematical end point $q^2 = q^2_{\text{max}} \simeq 0.129$ GeV^2.

We perform a combined fit of the q^2-, $m_{\ell'}$- and a-dependencies of the form factors using either the SU(2) ChPT inspired prediction proposed in Ref. [41] or a modified z-expansion. In both cases, we include the constraint arising from the CT theorem [25], which relates the scalar form factor $f_0(q^2)$ calculated at the unphysical point $q^2 = q^2_{\text{CT}} = M_K^2 - M_\pi^2$ to the ratio of the leptonic decay constants f_K/f_π in the SU(2) chiral limit.

A. SU(2) ChPT inspired Ansatz

Following Ref. [41], we derive the first Ansatz based on SU(2) ChPT starting from the expansion of the NLO SU(3) ChPT predictions for the semileptonic form factors [39,40] in powers of the variable $x \equiv M_\pi^2/M_K^2$, keeping only the $\mathcal{O}(x)$, $\mathcal{O}(x \log x)$ and $\mathcal{O}(\log(1-s))$ terms, where $s \equiv q^2/M_K^2$. The result of the expansion can be cast in the following form,

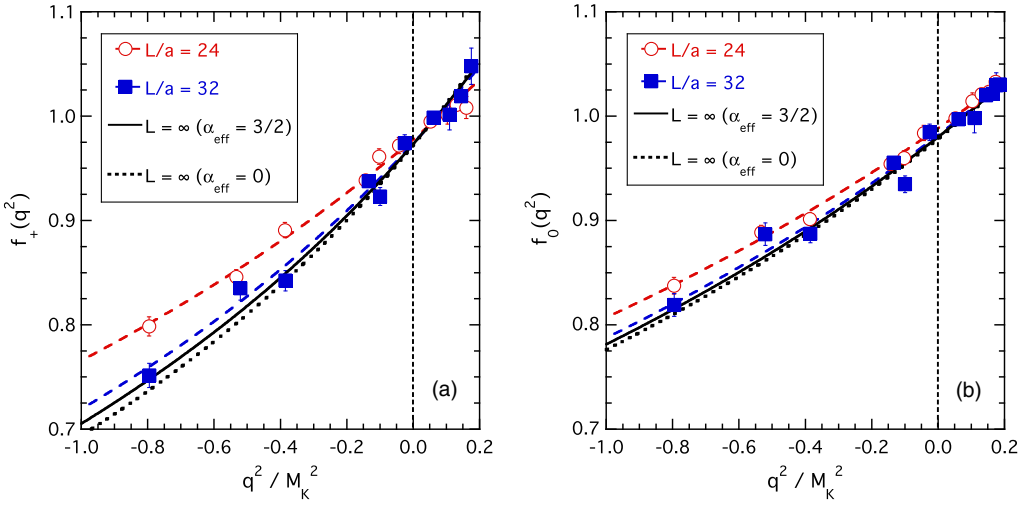

FIG. 5. Results for the vector (a) and scalar (b) form factors as functions of q^2/M_K^2 for the ensembles A40.24 and A40.32, which correspond to $\beta = 1.90$ and $M_\pi \simeq 300$ MeV at two different lattice volumes $L/a = 24$ (red dots) and $L/a = 32$ (blue squares), respectively. The dashed lines represent the results of a simple pole fit to the data for each lattice volume separately. The solid and dotted lines correspond to the infinite volume predictions obtained using Eq. (46) for the slopes in the two cases $\alpha_{\rm eff} = 0$ and $\alpha_{\rm eff} = 3/2$.

$$f_{+,0}(q^2) = F_+\left\{1 + C_+ x - \frac{M_K^2}{(4\pi f)^2}\left[\frac{3}{4}x\log x + xT_{+,0}^{(1)}(s) + T_{+,0}^{(2)}(s)\right]\right\} + \ldots, \tag{43}$$

with

$$\begin{aligned} T_+^{(1)}(s) &= [(1-s)\log(1-s) + s(1-s/2)]3(1+s)/4s^2, \\ T_+^{(2)}(s) &= [(1-s)\log(1-s) + s(1-s/2)](1-s)^2/4s^2, \\ T_0^{(1)}(s) &= [\log(1-s) + s(1+s/2)](9+7s^2)/4s^2, \\ T_0^{(2)}(s) &= [(1-s)\log(1-s) + s(1-s/2)] \\ &\quad \times (1-s)(3+5s)/4s^2. \end{aligned} \tag{44}$$

The coefficient of the pion chiral log in Eq. (43) is in agreement with the one predicted by SU(2) ChPT [38] both at $q^2 = 0$ and $q^2 = q^2_{\rm max}$. At $q^2 = 0$, the leading chiral log has the coefficient $(-3/4)$, while close to $q^2 = q^2_{\rm max}$, i.e., for $s \simeq (1-\sqrt{x})^2$, the function $T_0^{(1)}(s)$ contributes to the leading chiral log, obtaining for the scalar form factor $f_0(q^2_{\rm max})$ a final coefficient equal to $(-11/4)$ in agreement with Ref. [38].

As for the q^2-dependence, the results of the previous section suggest that a simple pole Ansatz is able to reproduce quite well the lattice data for each gauge ensemble [see Eq. (36)]. Note that the pole behavior is not predicted by either SU(3) or SU(2) ChPT at NLO [39,40], being a higher-order effect. Moreover, the slopes of the form factors $f_{+,0}(q^2)$ at $q^2 = 0$ [i.e., the parameters $1/M_{V,S}^2$ in Eq. (36)] determined for each gauge ensemble exhibit an almost linear dependence on the light-quark mass m_ℓ and on the squared lattice spacing a^2. In particular, as expected from the vector meson dominance model, the slope of the vector form factor extrapolated at the physical point is found to be consistent with the location of the physical $K^*(892)$ resonance.

Thus, our Ansatz for the vector and scalar form factors, inspired by SU(2) ChPT, has the following form,

$$f_{+,0}(q^2) = \frac{f_+^{SU(2)}(0) - F_+[xT_{+,0}^{(1)}(s) + T_{+,0}^{(2)}(s)]M_K^2/(4\pi f)^2}{1 - q^2[1 + P_{+,0}M_\pi^2 + D_{+,0}a^2 + K_{+,0}^{FSE}(L)]/\overline{M}_{V,S}^2} \times (1 + A_{+,0}s), \tag{45}$$

where $f_+^{SU(2)}(0)$ is given by Eq. (37), $\overline{M}_V$ is a parameter taken to be equal to the mass of the vector $K^*(892)$ resonance, and $\overline{M}_S$ is left as a free parameter in the fit. In Eq. (45), the quantity $K_{+,0}^{FSE}(L)$ is a phenomenological term that parametrizes the FSEs, which will be described soon, while $P_{+,0}$, $D_{+,0}$, $A_{+,0}$ and F_+ are free parameters. In order to improve the fit quality, we have inserted in the numerator of Eq. (45) an extra q^2-dependence through the factor $(1 + A_{+,0}s)$.

B. Finite size effects

FSEs have been investigated by comparing the results obtained for the two ensembles A40.24 and A40.32, which share the same lattice spacing and pion masses at different lattice volumes. The comparison is illustrated in Fig. 5, which shows the presence of sizeable FSEs in the slopes of the form factors with a larger impact in the case of the vector form factor. Instead, FSEs do not exceed ~1 standard deviation for the form factor at $q^2 = 0$. We remind the reader that FSEs are expected to be maximal for the ensemble A40.24.

The lattice data for the two volumes can be fitted by a simple pole Ansatz at each lattice volume separately (see the dashed lines in Fig. 5). This, however, cannot tell us anything about the infinite volume limit. To this end, we include FSEs on the slopes of the form factors $f_{+,0}(q^2)$ at $q^2 = 0$ by introducing the following phenomenological parametrization,

$$K^{\rm FSE}_{+,0}(L) = D^{\rm FSE}_{+,0} M_\pi^2 \frac{e^{-M_\pi L}}{(M_\pi L)^{\alpha_{\rm eff}}}, \tag{46}$$

where $D^{\rm FSE}_{+,0}$ are free parameters and $\alpha_{\rm eff}$ is an effective power that controls the decrease of FSEs at large values of $M_\pi L$. In the case $\alpha_{\rm eff} = 3/2$, the term $e^{-M_\pi L}/(M_\pi L)^{3/2}$ is known to represent the leading FSE correction to the pion mass and decay constant for $M_\pi L \gg 1$ [43].

In Fig. 5, we have given the predictions at infinite volume obtained using Eq. (46) for the slopes in the two cases $\alpha_{\rm eff} = 0$ and $\alpha_{\rm eff} = 3/2$. It can be seen that in both cases, the predictions at infinite volume are consistent with the data at the largest volume. The spread between the results obtained using $\alpha_{\rm eff} = 0$ and $\alpha_{\rm eff} = 3/2$ will be used to estimate the systematic uncertainty related to FSEs.

C. Modified z-expansion Ansatz

The second Ansatz for describing the q^2-, m_ℓ- and a-dependencies of the form factors is a modified version of the z-expansion given by Eq. (36), in which we take into account, as in Eq. (45), that the slopes of the form factors at $q^2 = 0$ have an almost linear dependence on the (renormalized) light-quark mass m_ℓ and on the squared lattice spacing a^2. We write

$$f_{+,0}(q^2) = \frac{f_+^{\rm SU(3)}(0) + \tilde{A}_{+,0}(z - z_0)[1 + (z + z_0)/2]}{1 - q^2(1 + \tilde{P}_{+,0} M_\pi^2 + \tilde{D}_{+,0} a^2 + \tilde{K}^{\rm FSE}_{+,0})/\tilde{M}^2_{V,S}}, \tag{47}$$

where $f_+^{\rm SU(3)}(0)$ is given by Eqs. (38)–(41), $\tilde{M}_V$ is a parameter taken to be equal to the mass of the vector $K^*(892)$ resonance, and $\tilde{M}_S$ is left as a free parameter in the fit.

We include in our analysis the constraint coming from the CT theorem [25], which states that the scalar form factor $f_0(q^2)$ at the (unphysical) CT point $q^2 = q^2_{\rm CT} = M_K^2 - M_\pi^2$ differs from the ratio of the leptonic decay constants f_K/f_π by terms which are proportional to the light-quark mass, namely $f_0(q^2 = M_K^2 - M_\pi^2) = f_K/f_\pi + \mathcal{O}(m_\ell)$. Therefore, in the SU(2) chiral limit, the scalar form factor $f_0(q^2)$ at $q^2 = q^2_{\rm CT} = q^2_{\rm max} = \overline{M}_K^2$ coincides with the ratio of the leptonic decay constants $\overline{f}_K/f$, where $\overline{f}_K$ and $\overline{M}_K$ are the SU(2) chiral limits of f_K

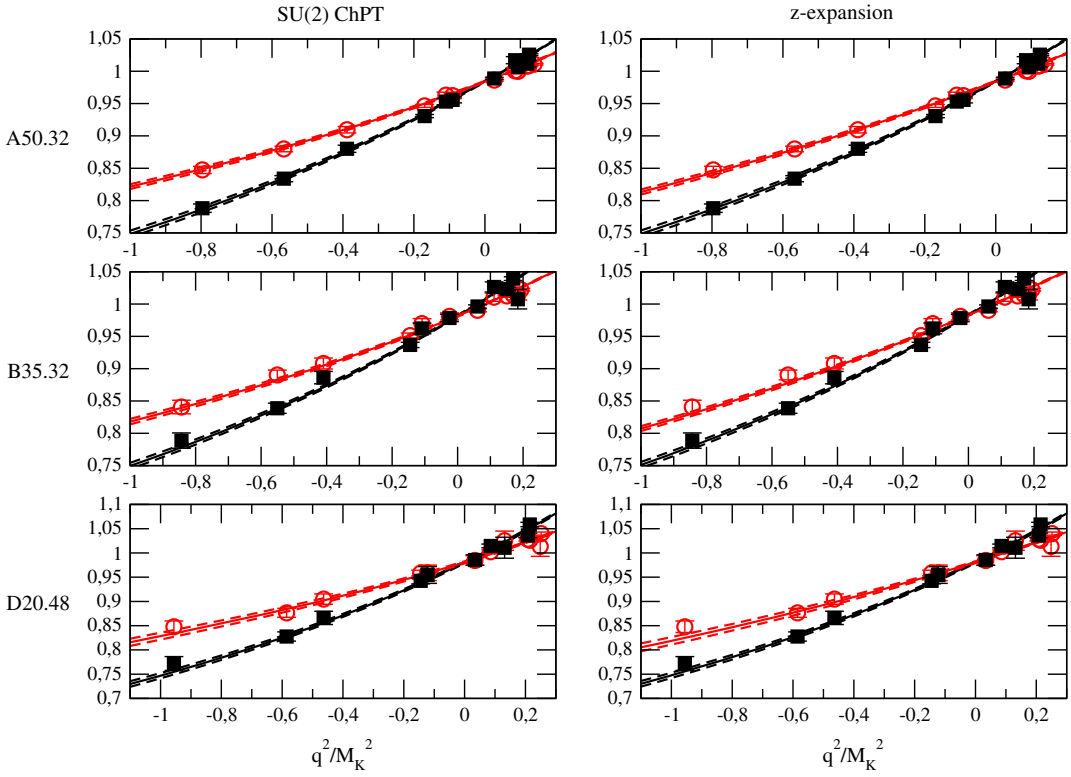

FIG. 6. Vector (black squares) and scalar (red circles) form factors vs q^2/M_K^2 for the ensembles A50.32, B35.32 and D20.48. The solid lines represent the results of the SU(2) ChPT (right panel) and the modified z-expansion (left panel) fits (see the text). The dashed lines identify the uncertainties due to the statistical errors of the data and to the fitting procedure.

and M_K, respectively. The CT theorem is therefore equivalent to impose on the parameters of Eqs. (45) and (47) the following constraints,

$$F_+ \frac{1+A_0}{1-\overline{M}_K^2/\overline{M}_S^2} = \frac{\overline{f}_K}{f} \qquad \text{[SU(2) ChPT inspired fit]},$$
$$\frac{1+\overline{f}_2+\Delta_0-2\tilde{A}_0}{1-\overline{M}_K^2/\tilde{M}_S^2} = \frac{\overline{f}_K}{f} \qquad \text{[mdodified } z\text{-expansion fit]}, \tag{48}$$

where $\overline{f}_2$ is the SU(2) chiral limit of Eq. (39) and the value for the ratio $\overline{f}_K/f$ is taken from the determination performed in Ref. [15].

Taking into account the constraints coming from the CT theorem, the number of free parameters for the SU(2) and modified z-expansion fits is 11 and 14, respectively. Generally speaking, all these parameters are functions of the strange quark mass, which, however, is fixed in our analysis at its physical value.

The quality of both the SU(2) ChPT and the modified z-expansion fits to our data is quite good, and it is illustrated in Fig. 6 in the cases of the three ensembles A50.32, B35.32 and D20.48.

The good scaling behavior of our lattice data for the vector and scalar form factors is illustrated in Fig. 7, where we have shown the results obtained after a small interpolations at the reference value $m_\ell = 20$ MeV for the light-quark mass and at few reference values of the variable q^2/M_K^2. The data depend mildly on a^2, and the discretization effects do not exceed the permille level.

In Table IV, we provide a set of synthetic data points with the corresponding total uncertainties representing our results

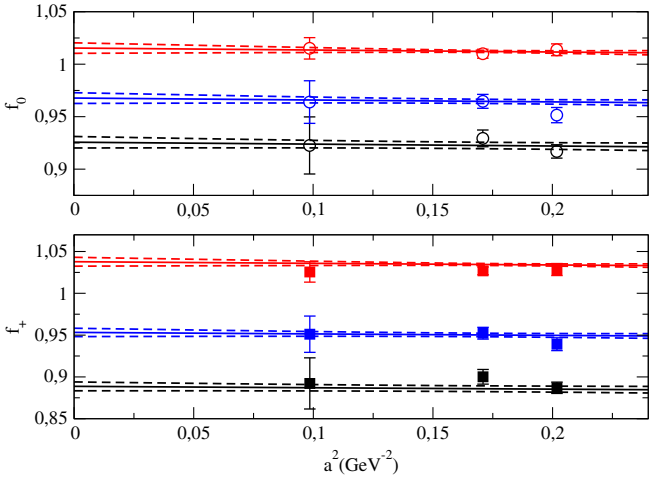

FIG. 7. Scaling behavior of the vector (squares) and scalar (circles) form factors, interpolated at the references values $m_\ell = 20$ MeV, $m_s = 99.6$ MeV and $q^2/M_K^2 = -0.33, -0.11, 0.14$ corresponding to black, blue and red markers (or bottom to top), respectively. Solid and dashed lines represent the results of the SU(2) ChPT fit with its statistical uncertainty.

TABLE IV. Synthetic data points representing our results for the vector and scalar form factors extrapolated to the physical pion point and in the continuum and infinite volume limits for 12 selected values of q^2 in the range between $q^2 = -q^2_{\rm max}$ and $q^2 = q^2_{\rm max}$, where $q^2_{\rm max} \simeq 0.129$ GeV^2 is the physical kinematical end point. The errors correspond to the combination in quadrature of both statistical and systematic errors (see the text).

q^2(GeV^2)	$f_+(q^2)$	$f_0(q^2)$
−0.1290	0.8288(81)	0.8911(100)
−0.0968	0.8603(72)	0.9097(86)
−0.0645	0.8943(62)	0.9290(72)
−0.0323	0.9311(53)	0.9494(59)
0.0	0.9711(47)	0.9711(47)
+0.0184	0.9954(47)	0.9840(42)
+0.0369	1.0211(49)	0.9976(37)
+0.0553	1.0480(55)	1.0117(35)
+0.0737	1.0764(64)	1.0264(36)
+0.0922	1.1062(76)	1.0419(42)
+0.1106	1.1378(90)	1.0581(52)
+0.1290	1.1711(106)	1.0753(67)

for the vector and scalar form factors, extrapolated to the physical pion mass and to the continuum and infinite volume limits, for 12 selected values of q^2 in the range between $q^2 = -q^2_{\rm max}$ and $q^2 = q^2_{\rm max}$ with $q^2_{\rm max} \simeq 0.129$ GeV^2.

The uncertainties correspond to the combination in quadrature of both statistical and systematic errors. These errors take into account (always in quadrature) the uncertainties induced by (i) the statistical noise and the fitting procedure; (ii) the errors present in the determination of the input parameters used in our analysis, namely the values of the average u/d quark mass m_{ud}, the lattice spacing a and the SU(2) ChPT LEC's f and B, determined in Ref. [14]; (iii) the chiral extrapolation, evaluated as half of the difference of the results obtained using the SU(2) ChPT and the modified z-expansion fits; iv) FSEs, evaluated by comparing the results obtained using the FSE factor (46) with $\alpha_{\rm eff} = 0$ and $\alpha_{\rm eff} = 3/2$, and v) discretization effects, calculated by comparing with the results obtained including in the denominator of Eqs. (45) and (47) a term proportional to $(a/r_0)^4$ and adopting for its coefficient a prior distribution equal to 0 ± 3.

D. Dispersive parametrization

In order to fit the q^2-dependence of our synthetic data points, we have used the same parametrization adopted in the analyses of the experimental data [2,10], namely the dispersive parametrization of Ref. [44], which reads

$$f_+^{\rm disp}(q^2) = f_+(0) e^{\frac{q^2}{M_\pi^2}[\Lambda_+ + H(q^2)]}, \tag{49}$$

$$f_0^{\rm disp}(q^2) = f_+(0) e^{\frac{q^2}{q^2_{\rm CT}}[\log(C) - G(q^2)]}, \tag{50}$$

where the dispersive functions $H(q^2)$ and $G(q^2)$ are given by

$$H(q^2) \equiv \frac{M_\pi^2 q^2}{\pi} \int_{q^2_{\rm cut}}^{\infty} ds \frac{\phi_+(s)}{s^2(s-q^2-i\varepsilon)}, \tag{51}$$

$$G(q^2) \equiv \frac{q^2_{\rm CT}(q^2_{\rm CT}-q^2)}{\pi} \int_{q^2_{\rm cut}}^{\infty} ds \frac{\phi_0(s)}{s(s-q^2_{\rm CT})(s-q^2-i\varepsilon)} \tag{52}$$

with $q^2_{\rm cut} \equiv (M_K + M_\pi)^2$. The parameters Λ_+ and C represent the slope of the vector form factor $f_+(q^2)$ at $q^2 = 0$ (in units of M_π^2) and the value of the scalar form factor $f_0(q^2)$ at the CT point $q^2 = q^2_{\rm CT} \equiv M_K^2 - M_\pi^2$ divided by $f_+(0)$, respectively. In Eqs. (51)–(52), the quantities ϕ_+ and ϕ_0 can be identified in the elastic region with the P-wave and S-wave phase shifts of the $(K\pi)_{I=1/2}$ scattering. The functions $H(q^2)$ and $G(q^2)$ have been estimated numerically in Ref. [44] with a $\simeq$10% accuracy, and their contributions do not exceed $\simeq$20% of the value of Λ_+ and $\log(C)$, respectively.

After performing a Taylor expansion of the form factors (49)–(50), viz.

$$f^{\rm disp}_{+,0}(q^2) = f_+(0)\left\{1 + \lambda'_{+,0}\frac{q^2}{M_\pi^2} + \frac{1}{2}\lambda''_{+,0}\left(\frac{q^2}{M_\pi^2}\right)^2 + \frac{1}{6}\lambda'''_{+,0}\left(\frac{q^2}{M_\pi^2}\right)^3 + \cdots\right\}, \tag{53}$$

one has [44]

$$\begin{aligned}
\lambda'_+ &= \Lambda_+, \\
\lambda''_+ &= (\lambda'_+)^2 + 5.79(97) \times 10^{-4}, \\
\lambda'''_+ &= (\lambda'_+)^3 + 5.79(97) \times 10^{-4} 3\lambda'_+ + 2.99(21) \times 10^{-5}
\end{aligned} \tag{54}$$

and

$$\begin{aligned}
\lambda'_0 &= \frac{M_\pi^2}{q^2_{\rm CT}}[\log(C) - 0.0398(44)], \\
\lambda''_0 &= (\lambda'_0)^2 + 4.16(56) \times 10^{-4}, \\
\lambda'''_0 &= (\lambda'_0)^3 + 4.16(56) \times 10^{-4} 3\lambda'_0 + 2.72(21) \times 10^{-5}.
\end{aligned} \tag{55}$$

We have applied the dispersive parametrization (53)–(55) to the synthetic data points of Table IV, having three parameters to be determined, namely the form factor $f_+(0)$, the vector slope Λ_+ and the logarithm of the scalar form factor at the CT point divided by $f_+(0)$, $\log(C)$. Using our bootstrap samples, which allow us to properly take into account the correlations among the synthetic data points, we have obtained

TABLE V. Sources of uncertainty in the final results (56)–(58) for the vector form factor $f_+(0)$ and the parameters Λ_+ and $\log(C)$ of the dispersive fit (53)–(55) performed using the synthetic data of Table IV at the physical point.

Uncertainty	$f_+(0)$	$\Lambda_+ \cdot 10^3$	$\log(C)$
Statistics + fitting procedure	0.0044	1.05	0.0133
Input parameters [14]	0.0011	0.44	0.0036
Chiral extrapolation	0.0009	0.17	0.0015
$a^2 \to 0$ extrapolation	0.0003	0.13	0.0002
Finite volume correction	0.0001	0.12	0.0002
Total	0.0046	1.16	0.0138

$$f_+(0) = 0.9709(44)_{\rm stat+fit}(11)_{\rm input}(9)_{\rm syst} = 0.9709(46), \tag{56}$$

$$\begin{aligned}
\Lambda_+ &= 24.22(1.05)_{\rm stat+fit}(0.44)_{\rm input}(0.25)_{\rm syst} \times 10^{-3} \\
&= 24.22(1.16) \times 10^{-3},
\end{aligned} \tag{57}$$

$$\log(C) = 0.1998(133)_{\rm stat+fit}(36)_{\rm input}(15)_{\rm syst} = 0.1998(138), \tag{58}$$

where all the uncertainties are combined in quadrature in the final error and the systematic error takes into account the uncertainties related to the chiral extrapolation, finite volume and discretization effects. The error budgets are given in Table V, and the correlation coefficients are equal to

$$\rho[f_+(0), \Lambda_+] = -0.228, \tag{59}$$

$$\rho[f_+(0), \log(C)] = -0.719, \tag{60}$$

$$\rho[\Lambda_+, \log(C)] = 0.376. \tag{61}$$

The result (56) for $f_+(0)$ is in nice agreement with the one of Eq. (42) obtained using the first strategy of our analysis (see Sec. III). Since it is slightly more precise, we take it as our final result for $f_+(0)$. Equation (56) is compatible with the current FLAG average $f_+(0) = 0.9661(32)$ at $N_f = 2+1$ [4], based on the results from FNAL/MILC [45] and RBC/UKQCD [46]. It is also consistent with the recent determinations $f_+(0) = 0.9704(24)_{\rm stat}(22)_{\rm syst} = 0.9704(32)$ from FNAL/MILC at $N_f = 2+1+1$ [6] and $f_+(0) = 0.9685(34)_{\rm stat}(14)_{\rm syst} = 0.9685(37)$ from RBC/UKQCD at $N_f = 2+1$ [7].

Finally, our results (57)–(58) compare positively with the corresponding updated FlaviaNet average of experimental results obtained in Ref. [10]:

$$\Lambda_+^{\rm exp} = 25.75(36) \times 10^{-3}, \tag{62}$$

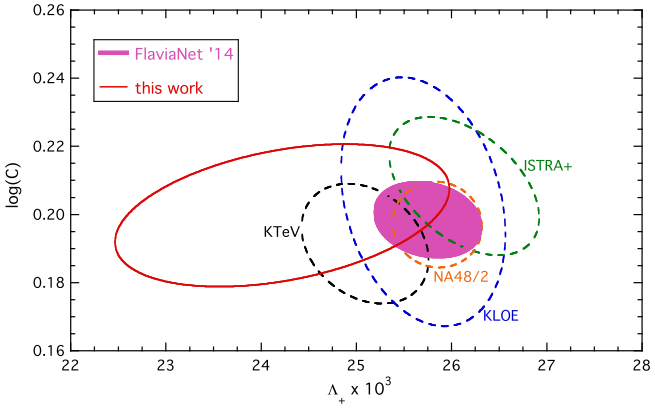

FIG. 8. Comparison of the information for the dispersive parameters Λ_+ and $\log(C)$ obtained in this work (solid ellipse) with the results of the $K_{\ell 3}$ experiments KTeV, KLOE, NA48/2 and ISTRA+ (dashed ellipses), taken from Refs. [2,10], and with the updated FlaviaNet average of Ref. [10] (full ellipse). All the ellipses represent contours corresponding to a 68% likelihood.

$$\log(C)^{\rm exp} = 0.1985(70). \tag{63}$$

The agreement is illustrated in Fig. 8, where the (68% likelihood) contour corresponding to our results (57)–(58), taking into account the correlation coefficient (61), is compared with the corresponding information coming from various $K_{\ell 3}$ experiments (taken from Refs. [2,10]) and with the updated FlaviaNet average of Ref. [10].

The momentum dependence of the vector and scalar form factors obtained from our dispersive fits can be inferred from Fig. 9, where the results for $f_{+,0}(q^2)$ are multiplied by $|V_{us}| = 0.2230$ [see Eq. (64) later] and compared with those obtained in Ref. [10] by applying the dispersive parametrization of Refs. [44,47] to the experimental data.

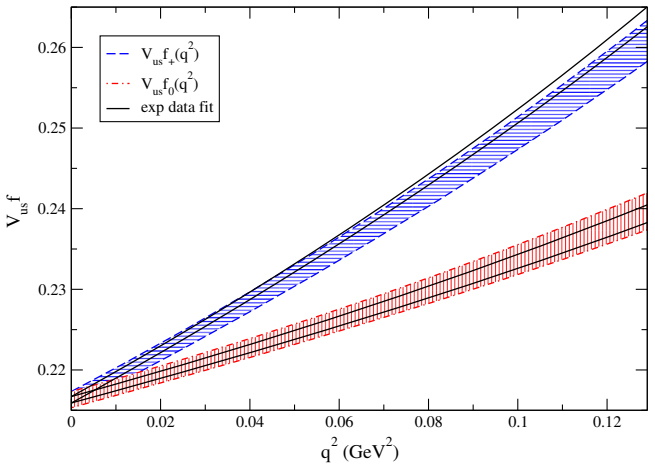

FIG. 9. Results for the vector (blue area) and scalar (red area) form factors, obtained at the physical point including both statistical and systematic uncertainties (see the text), multiplied by $|V_{us}| = 0.2230$ [see Eq. (64)] vs q^2 in the range between $q^2 = 0$ and the physical kinematical end point $q^2 = q^2_{\rm max} \simeq 0.129$ GeV^2. The black solid lines represent the results of the dispersive fit of the experimental data performed in Ref. [10].

The agreement with the experimental data shown in Figs. 8 and 9 is remarkable in spite of the larger uncertainties affecting the theoretical results. This provides a strong motivation for future investigations of the semileptonic vector and scalar form factors, which will improve the precision of the theoretical predictions not only at the particular kinematical point $q^2 = 0$ but in the full q^2-range covered by the experiments, obtaining in this way a more stringent test of the SM in $K_{\ell 3}$ decays.

In order to allow a direct use of the synthetic data points without using our bootstrap samples, we have calculated the covariance matrix among the synthetic data points of Table IV. Its dimension is 23×23, and it cannot be easily given in tables. We can therefore supply it upon request.

V. EVALUATION OF $|V_{us}|$

Combining our final result (56) for the vector form factor $f_+(0)$ with the experimental value of $|V_{us}|f_+(0) = 0.2165(4)$ from Ref. [10], we can estimate the CKM matrix element $|V_{us}|$, obtaining

$$|V_{us}| = 0.2230(4)_{\rm exp}(11)_{f_+(0)} = 0.2230(11) \quad \text{from } K_{\ell 3} \text{ decays}, \tag{64}$$

where the errors come from experiments and from the lattice computation, respectively.

The result (64) may be compared with the determination of $|V_{us}|$ coming from the ratio of the kaon and pion leptonic decay constants $f_{K^+}/f_{\pi^+} = 1.184(16)$, obtained in Ref. [15] using the same ETM Collaboration gauge configurations for the lattice calculations. Taking the updated value of $|V_{ud}| = 0.97417(21)$ from the superallowed nuclear β decay [23] and the updated experimental value of $|V_{us}/V_{ud}|f_{K^+}/f_{\pi^+} = 0.2760(4)$ from Ref. [10], one gets

$$|V_{us}| = 0.2271(29) \quad \text{from } K_{\ell 2} \text{ decays}, \tag{65}$$

which is in slight tension (~1.3 standard deviations) with the result (64) obtained from $K_{\ell 3}$ decays.[5] We can also use our results (64)–(65) to test the unitarity of the first row of the CKM matrix using the updated PDG value of $|V_{ub}| = 0.00413(49)$ from B-meson decays [24]. One obtains

[5]The slight tension among the results (64)–(65) is not significantly changed by the small correlation coefficient occurring between our result (56) for $f_+(0)$ and the ETM Collaboration value of f_{K^+}/f_{π^+} obtained in Ref. [15].

$$|V_{ud}|^2+|V_{us}|^2+|V_{ub}|^2=0.99875(64) \quad \text{from } K_{\ell 3} \text{ decays},$$
$$|V_{ud}|^2+|V_{us}|^2+|V_{ub}|^2=1.0008(14) \quad \text{from } K_{\ell 2} \text{ decays}, \tag{66}$$

which test the first-row unitarity at the permille level for the $K_{\ell 2}$ decays and even below for the $K_{\ell 3}$ modes. In the latter case, a slight tension with unitarity at the level of ~ 2 standard deviations is observed.

VI. CONCLUSIONS

We present a new lattice QCD determination of the vector and scalar form factors of the semileptonic $K \to \pi \ell \nu$ decay which are relevant for the extraction of the CKM matrix element $|V_{us}|$ from experimental data.

Our results are based on the gauge configurations produced by the European Twisted Mass Collaboration with $N_f = 2+1+1$ dynamical fermions, which include in the sea, besides two light mass degenerate quarks, also the strange and the charm quarks. Using data simulated at three different values of the lattice spacing and with pion masses as small as 210 MeV, our final result for the vector form factor at zero momentum transfer is

$$f_+(0) = 0.9709(44)_{\text{stat+fit}}(11)_{\text{input}}(9)_{\text{syst}} = 0.9709(46), \tag{67}$$

where all the uncertainties are combined in quadrature in the final error.

Using the latest experimental value of $f_+(0)|V_{us}|$ from $K_{\ell 3}$ decays [10], we obtain

$$|V_{us}| = 0.2230(11). \tag{68}$$

This allows us to test the unitarity constraint of the Standard Model below the permille level once the determination of V_{ud} from superallowed nuclear β decays is adopted, namely

$$|V_{ud}|^2+|V_{us}|^2+|V_{ub}|^2 = 0.99875(64), \tag{69}$$

which highlights also a slight tension with unitarity at the level of ~ 2 standard deviations.

Besides $f_+(0)$, we have determined from our lattice data the values of the parameters Λ_+ and $\log(C)$ appearing in the dispersive parametrization (53)–(55), which is adopted also to describe the experimental data [2,10]. Our results are given in Eqs. (57) and (58) and compare positively with the corresponding latest experimental results (62)–(63) from Ref. [10]. The consistency with the information coming from various $K_{\ell 3}$ experiments [2,10] is remarkable, as shown in Fig. 8.

We have also presented our results for the semileptonic scalar $f_0(q^2)$ and vector $f_+(q^2)$ form factors in the whole range of values of the squared 4-momentum transfer q^2 measured in $K_{\ell 3}$ decays, obtaining a very good agreement with the momentum dependence of the experimental data, as illustrated in Fig. 9.

Our findings represent a strong motivation for future investigations of the semileptonic vector and scalar form factors, which will improve the precision of the theoretical predictions not only at the particular kinematical point $q^2 = 0$, but in the full q^2-range covered by the experiments, obtaining in this way a more stringent test of the Standard Model in $K_{\ell 3}$ decays.

Finally, we have provided a set of synthetic data points representing our results for the vector and scalar form factors at the physical point for selected values of q^2 in the range between $q^2 = 0$ and the physical end point $q^2 \simeq 0.129$ GeV^2 (including the covariance matrix for the data at different values of q^2, which is available upon request).

ACKNOWLEDGMENTS

We thank our colleagues of the ETM Collaboration for fruitful discussions. We acknowledge the CPU time provided by the PRACE Research Infrastructure under Project No. PRA027 "QCD Simulations for Flavor Physics in the Standard Model and Beyond" on the JUGENE BG/P system at the Jülich SuperComputing Center (Germany) and by the agreement between INFN and CINECA under the specific initiatives INFN-RM123 and INFN-LQCD123 on the BG/Q system Fermi at CINECA (Italy). V. L., S. S. and C. T. thank MIUR (Italy) for partial support under Contract No. PRIN 2010-2011. L. R. thanks INFN (Italy) for the support under the Super Massive (SUMA) computing project (https://web2.infn.it/SUMA).

[1] N. Cabibbo, Phys. Rev. Lett. **10**, 531 (1963); M. Kobayashi and T. Maskawa, Prog. Theor. Phys. **49**, 652 (1973).
[2] M. Antonelli *et al.* (FlaviaNet Working Group on Kaon Decays Collaboration), Eur. Phys. J. C **69**, 399 (2010).
[3] G. Colangelo *et al.*, Eur. Phys. J. C **71**, 1695 (2011).
[4] S. Aoki *et al.*, Eur. Phys. J. C **74**, 2890 (2014).
[5] D. Bećirević, G. Isidori, V. Lubicz, G. Martinelli, F. Mescia, S. Simula, C. Tarantino, and G. Villadoro, Nucl. Phys. **B705**, 339 (2005).
[6] A. Bazavov *et al.*, Phys. Rev. Lett. **112**, 112001 (2014).
[7] P. A. Boyle *et al.* (RBC/UKQCD Collaboration), J. High Energy Phys. 06 (2015) 164.

[8] R. Baron *et al.* (ETM Collaboration), J. High Energy Phys. 06 (2010) 111.
[9] R. Baron *et al.* (ETM Collaboration), *Proc. Sci.*, LATTICE2010 (2010) 123.
[10] M. Moulson, arXiv:1411.5252.
[11] L. Riggio *et al.* (ETM Collaboration), *Proc. Sci.*, LATTICE2014 (2014) 387.
[12] N. Carrasco, P. Lami, V. Lubicz, E. Picca, L. Riggio, S. Simula, and C. Tarantino, arXiv:1410.7159.
[13] N. Carrasco, P. Lami, V. Lubicz, L. Riggio, and S. Simula, arXiv:1511.04880.
[14] N. Carrasco *et al.*, Nucl. Phys. **B887**, 19 (2014).
[15] N. Carrasco *et al.*, Phys. Rev. D **91**, 054507 (2015).
[16] Y. Iwasaki, Nucl. Phys. **B258**, 141 (1985).
[17] R. Frezzotti and G. C. Rossi, Nucl. Phys. B, Proc. Suppl. **128**, 193 (2004).
[18] R. Frezzotti and G. C. Rossi, J. High Energy Phys. 08 (2004) 007.
[19] R. Frezzotti and G. C. Rossi, J. High Energy Phys. 10 (2004) 070.
[20] K. Osterwalder and E. Seiler, Ann. Phys. (N.Y.) **110**, 440 (1978).
[21] R. Sommer, Nucl. Phys. **B411**, 839 (1994).
[22] M. Constantinou *et al.* (ETM Collaboration), J. High Energy Phys. 08 (2010) 068.
[23] J. C. Hardy and I. S. Towner, Phys. Rev. C **91**, 025501 (2015).
[24] K. A. Olive *et al.* (Particle Data Group Collaboration), Chin. Phys. C **38**, 090001 (2014).
[25] C. G. Callan and S. B. Treiman, Phys. Rev. Lett. **16**, 153 (1966).
[26] C. McNeile and C. Michael (UKQCD Collaboration), Phys. Rev. D **73**, 074506 (2006).
[27] R. Frezzotti, V. Lubicz, and S. Simula (ETM Collaboration), Phys. Rev. D **79**, 074506 (2009).
[28] P. F. Bedaque, Phys. Lett. B **593**, 82 (2004).
[29] G. M. de Divitiis, R. Petronzio, and N. Tantalo, Phys. Lett. B **595**, 408 (2004).
[30] D. Guadagnoli, F. Mescia, and S. Simula, Phys. Rev. D **73**, 114504 (2006).
[31] J. M. Flynn, A. Jüttner, and C. T. Sachrajda (UKQCD Collaboration), Phys. Lett. B **632**, 313 (2006).
[32] P. A. Boyle, J. M. Flynn, A. Juttner, C. T. Sachrajda, and J. M. Zanotti, J. High Energy Phys. 05 (2007) 016.
[33] P. A. Boyle, J. M. Flynn, A. Jüttner, C. Kelly, C. Maynard, H. Pedroso de Lima, C. T. Sachrajda, and J. M. Zanotti (RBC-UKQCD Collaboration), Eur. Phys. J. C **69**, 159 (2010).
[34] V. Lubicz, F. Mescia, S. Simula, and C. Tarantino (ETM Collaboration), Phys. Rev. D **80**, 111502 (2009).
[35] C. T. Sachrajda and G. Villadoro, Phys. Lett. B **609**, 73 (2005).
[36] P. F. Bedaque and J. W. Chen, Phys. Lett. B **616**, 208 (2005).
[37] C. Bourrely, I. Caprini, and L. Lellouch, Phys. Rev. D **79**, 013008 (2009); **82**, 099902(E) (2010).
[38] J. M. Flynn, and C. T. Sachrajda (RBC and UKQCD Collaborations), Nucl. Phys. **B812**, 64 (2009).
[39] J. Gasser and H. Leutwyler, Nucl. Phys. **B250**, 517 (1985).
[40] J. Gasser and H. Leutwyler, Nucl. Phys. **B250**, 465 (1985).
[41] V. Lubicz *et al.* (ETM Collaboration), *Proc. Sci.*, LATTICE2010 (2010) 316.
[42] M. Ademollo and R. Gatto, Phys. Rev. Lett. **13**, 264 (1964).
[43] J. Gasser and H. Leutwyler, Phys. Lett. B **184**, 83 (1987).
[44] V. Bernard, M. Oertel, E. Passemar, and J. Stern, Phys. Rev. D **80**, 034034 (2009).
[45] A. Bazavov *et al.*, Phys. Rev. D **87**, 073012 (2013).
[46] P. A. Boyle, J. M. Flynn, N. Garron, A. Jttner, C. T. Sachrajda, K. Sivalingam, and J. M. Zanotti, J. High Energy Phys. 08 (2013) 132.
[47] V. Bernard, M. Oertel, E. Passemar, and J. Stern, Phys. Lett. B **638**, 480 (2006).